Magnetic droplet solitons in orthogonal nano-contact spin torque oscillators

S. M. Mohseni[1,2,*], S. R. Sani[1,2], R. K. Dumas[3], J. Persson[2], T. N. Anh Nguyen[1], S. Chung[1,3], Ye. Pogoryelov[3], P. K. Muduli[3,4], E. Iacocca[3], A. Eklund[5], and J. Åkerman[1,2,3]

[1]*Materials Physics, School of ICT, Royal Institute of Technology, Electrum 229, 164 40 Kista, Sweden*

[2]*NanOsc AB, Electrum 205, 164 40 Kista, Sweden*

[3]*Department of Physics, University of Gothenburg, 412 96 Gothenburg, Sweden*

[4]*Department of Physics, Indian Institute of Technology Delhi, New Delhi, 110016, India*

[5]*Devices and Circuits, School of ICT, Royal Institute of Technology, Electrum 229, 164 40 Kista, Sweden*

Abstract

We study microwave signal generation as a function of drive current and applied perpendicular magnetic field in nano-contact spin torque oscillators (NC-STOs) based on orthogonal (pseudo) spin valves where the Co fixed layer has a strong easy-plane anisotropy, and the [Co/Ni] free layer has a strong perpendicular magnetic anisotropy. The orthogonal NC-STOs exhibit a dramatic transition from the conventional ferromagnetic resonance-like spin wave mode to a magnetic droplet soliton mode. In particular, the field and current dependence of the droplet soliton near threshold are discussed. Near threshold the droplet soliton undergoes complex dynamics that include mode hopping, as evident in the experimental frequency domain and magnetoresiatance response.

[*]Corresponding author email address: majidm@kth.se

Introduction

The classic spin torque [1-3] oscillator (STO) [4] architecture relies on a spin valve (SV) structure where a significant spin polarization is generated by a reference layer (RL) and the dynamical processes occur in a nearby free layer (FL). Both nano-pillar [5], where the lateral cross section of the entire SV stack has been reduced to a typically <100 nm diameter, and nanocontact (NC), [6,7] where only the current injection site has been laterally defined, designs have been implemented. Owing to their extended FL, NC-STOs hold particular promise as spin wave injectors for magnonic applications [8]. Many attractive properties including a large tuning range [9,10] and modulation rates [11-13] were initially realized in devices utilizing materials with in-plane (IP) anisotropy in both the RL and FL. Unfortunately, large magnetic fields are typically required to reap the benefits of these devices. Low to zero field operation has been realized [14-16] in devices that combine materials with both IP and out-of-plane (OOP) anisotropy, at the cost of bandwidth and output power. These limitations may be overcome [17,18] by instead relying on materials [19-23] with tilted anisotropy. Yet another alternative was recently realized using an orthogonal SV structure with an IP RL and OOP FL, and demonstrated high frequency operation at low external fields [24,25]. The IP FL can be simply realized using either Co or CoFe alloys with high spin polarization and spin-torque efficiency. Owing to their tunable saturation magnetization (M_S) and perpendicular magnetic anisotropy (PMA), all magnetic Co/Ni multilayers [26] (MLs) have proven to be the ideal material for use as the OOP FL.

Furthermore, such orthogonal SV STOs have been shown to support a fundamentally new type of magnetic excitation, namely the magnetic droplet soliton. While the initial theoretical prediction by Ivanov and Kosevich [27], of a “magnon drop” soliton in thin films with PMA and zero damping dates back to the 1970s, more recent treatments by Hoefer *et al.* [28-29] demonstrated analytically that a related “magnetic droplet” soliton is possible to excite in NC-STOs. Here, the important criterion played by spin transfer torque is to locally realize the condition of zero-damping necessary for droplet formation. The droplet frequency, f_o, lies between the Zeeman frequency, f_{Zeeman}, and the ferromagnetic resonance (FMR) frequency, f_{FMR}. In this paper, we describe in detail the transition from the FMR-like spin wave mode to the

droplet soliton as a function of both applied field and current. In particular, the complex dynamics near this transition, including mode jumping, will be discussed.

Experimental

The orthogonal-pseudo spin valves (PSVs) were deposited by magnetron sputtering at room temperature on thermally oxidized Si substrates in a chamber with a base pressure better than 5×10^{-8} Torr. A slow sputtering growth rate was used for the ultra-thin Co and Ni to maximize uniformity and minimize inter-diffusion. A Ta(4 nm)/Cu(10 nm)/Ta(4 nm) trilayer with (111)-texture is used as a seed layer to maximize the PMA of the Co/Ni ML and to act as a low resistive base layer to minimize lateral current spreading under the NC in the final STO devices. The orthogonal-PSV has the following layer structure: Co(6 nm)/Cu(6 nm)/Co(0.2 nm)-[Ni(0.6 nm)/Co(0.25 nm)]$_4$, as schematically shown in Fig. 1. Here, the first thick Co(6 nm) layer has in-plane anisotropy and plays the role of the RL. The [Co/Ni] ML acts as the FL and has PMA. The number of ML, their thicknesses, and the Co/Ni thickness ratio were all optimized to obtain high PMA [30]. The magnetization response of [Co/Ni] ML exhibits a low out-of-plane saturation field, square hysteresis loop with nearly 100% remanence, and a coercivity of 200 Oe. This layer has $\mu_o M_S$=0.95 T and a hard axis, i.e. IP, saturation of $\mu_o(H_k\text{-}M_S)$=0.35 T. Finally, the ML stack is capped with Cu(2 nm)/Pd(2 nm) to prevent oxidation.

Fabrication of the NC-STOs begins by patterning the blanket films an 8×16 μm^2 mesa using optical lithography. This is followed by an insulating SiO_2 layer deposited by chemical vapor deposition. The NC area was defined using electron-beam lithography and reactive ion etching through the SiO_2, as schematically shown in Fig.1. Finally, a Cu(1.1 μm)/Au(100 nm) top electrode, forming a coplanar waveguide, was patterned using optical lithography, sputter deposition, and lift-off [31].

Electrical characterization [10] of the NC-STOs is performed in a custom probe station with variable current, magnetic field, and applied field angle capabilities. The DC current was fed to the device using a precision current source through a bias tee connected in parallel with the transmission line. The resulting RF signal is then amplified using a broadband microwave amplifier and finally analyzed in the frequency domain with a spectrum analyzer. The DC

voltage across the device was also recorded simultaneously for magnetoresistance (MR) measurements. Finally, all measurements are performed at room temperature and with the applied field perpendicular to the film plane.

Results and Discussion

The dynamics in similar orthogonal-PSVs have been extensively studied in low (<~0.4 T) perpendicular fields [24,25]. The nature of these dynamics are characterized by very small angle precessions, similar to FMR, as schematically represented in Fig. 1(a). The oscillation characteristics as a function of current, and several applied fields, for NC-STO with a NC diameter of 50 nm is shown in Fig. 2. The frequency of this FMR-like spin wave mode decreases as the magnitude of the applied current increases, i.e. redshifts, as the precession angle increases. For $\mu_o H$=0.03 and 0.2 T only the FMR-like mode is found. However, when the field is increased to 0.4 T a dramatic drop (~8 GHz) in frequency at I_{dc}=-3.6 mA is found corresponding to the transition from the FMR-like spin wave mode near to the droplet mode. As the applied field is increased beyond 0.4 to 1 T the FMR-like mode vanishes, and may drop below our experimental detection limit, and the strength of the droplet mode increases. Based on micromagnetic simulations [32], we see that the precession trajectory, as schematically represented in Fig. 1(b) is fundamentally different than the FMR-like mode. Here, the precession angle is largest near the boundary of the droplet and decreases towards the center. A curious dip in the frequency is also observed in Fig. 2. We speculate that the applied field, the Oersted field [33], and possibly coupling of free layer to the fixed layer magnetization through interlayer exchange coupling via the Cu spacer, all combine to modify the local energy landscape. Unfortunately this very complex interplay still needs further studies and understanding and is well beyond the scope of this paper.

Further analysis of the FMR-like to droplet mode transition is shown in Fig. 3. Both the FMR-like and droplet mode, and corresponding 2nd harmonic, can be clearly seen in the color map shown in Fig. 3(a). The dashed vertical dashed line $\mathbf{S_1}$, I_{dc}=-3.65 mA, is very near the mode transition and clearly shows, Fig. 3(a, upper inset), that both the FMR-like and droplet modes exist in the frequency domain. Near the mode transition, the power, Fig. 3(b), of the droplet mode is either lower, or comparable to the FMR-like mode. Additionally, the linewidth, Fig.

3(c), of the droplet mode is significantly larger than the FMR-like mode. This suggests that near the transition the droplet mode is not stable and perhaps there is mode-jumping between it and the FMR-like mode. However, far from the mode transition the power of the droplet mode, Fig. 3(b), is about one order of magnitude bigger than the droplet mode. Finally, once the droplet mode becomes stabilized, as highlighted with the vertical dashed line **S2** I_{dc}=-4.05 mA, the 2nd harmonic of the droplet mode becomes clearly visible, consistent with a precession trajectory that is not perfectly circular [24].

To map out in detail the transition from the FMR-like to droplet mode, the MR [ΔR=R(H)-R(H=0)] was recorded, shown as a 2-dimensional phase diagram in Fig. 4. The current and field where ΔR starts to sharply increase represents the point where the STO response changes from an FMR-like to droplet mode. For a 1-dimensional example, see the closed circles in Fig. 5 which shows droplet formation occurring at approximately $\mu_o H$=1.2 T. As the current increases, the necessary field to nucleate the droplet decreases, consistent with what was found in Ref. [32] for different NC sizes.

The results shown in Fig. 5 are for a device with a nominal NC diameter of 60 nm at I_{dc}=-5.6 mA, the minimum current necessary for droplet formation. As the applied field is increased the MR shows a steady decline as the alignment of the magnetization in the Co RL and [Co/Ni] ML FL become more parallel. However, a large positive jump in MR is seen at $\mu_o H$=1.12 T indicating stable droplet formation and more anti-parallel alignment between the Co RL and the reversed portion of the FL. After droplet formation the slope of the MR response now becomes positive as the alignment between the RL and FL slowly becomes progressively more anti-parallel. What is most interesting here is the complex transition region defined by the region between where the FMR-like mode disappears at $\mu_o H$=0.56 T and a stable droplet mode exists at $\mu_o H$=1.12 T. At $\mu_o H$=0.56 T a new mode appears with a frequency slightly below that of the FMR-like mode. This in accompanied by a very slight increase in the MR signal as compared to the FMR-like mode, therefore we believe this mode is related to a partially reversed droplet, as predicted by theory [28]. To be able to clearly resolve the increased MR we used a dashed yellow guiding line which represents the expected extension of the MR signal for the STO if the droplet was not nucleated. We refer to this mode as the 1st droplet mode in the Fig. 5. This mode exists for field <1 T. For the applied field ranges of 0.76 T< $\mu_o H$ < 0.9 T and 0.98 T< $\mu_o H$ < 1.08

T another droplet signal, referred to as the 2nd droplet mode, appears and is accompanied by a larger increase in MR as we expect this droplet to more fully reversed. The MR response should be interpreted as an average of the rapid mode-hopping and therefore has an intermediate MR. As was similarly observed in Fig. 3, near the FMR-like to droplet mode transition, multiple droplet modes can exist in the frequency domain and mode-hopping between the two is likely taking place near the onset of steady droplet formation.

Conclusions

The formation of a droplet soliton in orthogonal-STOs was discussed. Particular attention was paid to the FMR-like to droplet transition as a function of both DC current and applied field. We find that this transition is not necessarily sharp and includes more complicated dynamics and modes. As the magnitude of the bias current was increased evidence of mode-hopping between the FMR-like and droplet mode was found. Additionally, as the magnitude of the perpendicularly applied field was increased an even more complex transition is observed that not only includes formation of an unstable and partially reversed droplet soliton, but mode-hopping between it and the stable droplet soliton found at higher applied fields.

Acknowledgments

This work was supported by the EC FP7 Contract ICT-257159 “MACALO”, the Swedish Foundation for Strategic Research (SSF) program “Future Research Leaders”, the Swedish Research Council (VR), and the Knut and Alice Wallenberg Foundation. Johan Åkerman is a Royal Swedish Academy of Sciences Research Fellow supported by a grant from the Knut and Alice Wallenberg Foundation.

References

[1] L. Berger, Phys. Rev. B **54**, 9353 (1996).

[2] J. Slonczewski, J. Magn. Magn. Mater. **159**, L1 (1996).

[3] D. Ralph, M. Stiles, J. Magn. Magn. Mater. **320**, 1190 (2008).

[4] T. Silva, W. Rippard, J. Magn. Magn. Mater. **320**, 1260 (2008).

[5] S. I. Kiselev, J. C. Sankey, I. N. Krivorotov, N.C. Emley, R. J. Schoelkopf, R. A. Buhrman, D. C. Ralph, Nature **425**, 380 (2003).

[6] F. B. Mancoff, N. D. Rizzo, B. N. Engel, S. Tehrani, Nature **437**, 393 (2005).

[7] S. Kaka, M. R. Pufall, W. H. Rippard, T. J. Silva, S. E. Russek, J. A. Katine, Nature **437**, 389 (2005).

[8] M. Madami, S. Bonetti, G. Consolo, S. Tacchi, G. Carlotti, G. Gubbiotti, F. B. Mancoff, M. A. Yar, J. Åkerman, Nature Nanotech. **6**, 635 (2011).

[9] W. Rippard, M. Pufall, S. Kaka, S. Russek, T. Silva, Phys. Rev. Lett. **92**, 027201 (2004).

[10] S. Bonetti, P. Muduli, F. Mancoff, J. Åkerman, Appl. Phys. Lett. **94**, 102507 (2009).

[11] M. R. Pufall, W. H. Rippard, S. Kaka, T. J. Silva, and S. E. Russek, Appl. Phys. Lett. **86**, 082506 (2005).

[12] P. K. Muduli, Ye. Pogoryelov, S. Bonetti, G. Consolo, F. Mancoff, J. Åkerman, Phys. Rev. B **81**, 140408(R) (2010).

[13] P. K. Muduli, Ye. Pogoryelov, Y. Zhou, F. Mancoff, J. Åkerman, Integr. Ferroelectr. **125**, 147 (2011).

[14] T. Devolder, A. Meftah, K. Ito, J. A. Katine, P. Crozat, and C. Chappert, J. Appl. Phys. **101**, 063916 (2007).

[15] D. Houssameddine, U. Ebels, B. Delaët, B. Rodmacq, I. Firastrau, F. Ponthenier, M. Brunet, C. Thirion, J-P. Michel, L. Prejbeanu-Buda, M-C. Cyrille, O. Redon, B. Dieny, Nature Mater. **6**, 441 (2007).

[16] V. S. Pribiag, I. N. Krivorotov, G. D. Fuchs, P. M. Braganca, O. Ozatay, J. C. Sankey, D. C. Ralph, R. A. Buhrman, Nature Phys. **3**, 498 (2007).

[17] Yan Zhou, C. L. Zha, S. Bonetti, J. Persson, J. Åkerman, Appl. Phys. Lett. **92**, 262508 (2008).

[18] Y. Zhou, S. Bonetti, C. L. Zha, J. Åkerman, New J. Phys. **11**, 103028 (2009).

[19] T.N. Anh Nguyen, N. Benatmane, V. Fallahi, Y. Fang, S.M. Mohseni, R.K. Dumas, J. Åkerman, J. Magn. Magn. Mater. **324**, 3932 (2012).

[20] S. Chung, S. M. Mohseni, V. Fallahi, T. N. Anh Nguyen, N. Benatmane, R. K. Dumas, J. Åkerman, J. Phys. D: Appl. Phys. **46**, 125004 (2013).

[21] S. Tacchi, T. N. Anh Nguyen, G. Carlotti, G. Gubbiotti, M. Madami, R. K. Dumas, J. W. Lau, J. Åkerman, A. Rettori, M. G. Pini, Phys. Rev. B **87**, 144426 (2013).

[22] T. N. Anh Nguyen, Y. Fang, V. Fallahi, N. Benatmane, S. M. Mohseni, R. K. Dumas, J. Åkerman, Appl. Phys. Lett. **98**, 172502 (2011).

[23] C. L. Zha, J. Persson, S. Bonetti, Y. Fang, J. Åkerman, Appl. Phys. Lett. **94**, 163108 (2009).

[24] W. H. Rippard, A. M. Deac, M. R. Pufall, J. M. Shaw, M. W. Keller, S. E. Russek, C. Serpico, Phys. Rev. B **81**, 014426 (2010).

[25] S. M. Mohseni, S. R. Sani, J. Persson, T. N. Anh Nguyen, S. Chung, Ye. Pogoryelov, J. Åkerman, Phys. Status Solidi-RRL **5**, 432–434 (2011).

[26] S. M. Mohseni, R. K. Dumas, Y. Fang, J. Lau, S. Sani, J. Persson, J. Åkerman, Phys. Rev. B **84**, 174432 (2011).

[27] A.M. Kosevich, B.A. Ivanov, A.S. Kovalev, Phys. Rep. **194**, 117 (1990).

[28] M. Hoefer, T. Silva, and M. Keller, Phys. Rev. B **82**, 054432 (2010).

[29] M. Hoefer, M. Sommacal, T. Silva, Phys. Rev. B **85**, 214433 (2012).

[30] S.M. Mohseni, PhD thesis, KTH, ICT (December 2012).

[31] S.R. Sani, PhD thesis, KTH, ICT (June 2013).

[32] S. M. Mohseni, S. R. Sani, J. Persson, T. N. A. Nguyen, S. Chung, Y. Pogoryelov, P. K. Muduli, E. Iacocca, A. Eklund, R. K. Dumas, S. Bonetti, A. Deac, M. A. Hoefer, J. Akerman, Science **339**, 1295 (2013).

[33] R.K. Dumas, E. Iacocca, S. Bonetti, S.R. Sani, S.M. Mohseni, A. Eklund, J. Persson, O. Heinonen, and Johan Åkerman, Phys. Rev. Lett. **110**, 257202 (2013).

Figure captions

Fig. 1: A 2-dimensional schematic representation of the magnetization in the vicinity of the nanocontact for the (a) FMR-like mode with small angle precession at the center and (b) droplet mode with large angle precession at the NC boundary (b).

Fig. 2: STO operating frequency versus current at different fields. There are both FMR-like and droplet modes present at 0.4 T.

Fig. 3: (a) Current sweep of a NC with a diameter of 50 nm, measured at $\mu_0 H$=0.4 T. Insets S_1 and S_2 in the figure are indicated by vertical lines and show the spectra at -3.65 and -4.05 mA. Integrated power (b) and linewidth (c) are shown for each mode.

Fig. 4: A current-field phase diagram of ΔR, indicating changes from FMR-like mode to droplet mode. The boundary between two oscillation modes can be understood as an immediate increase in ΔR (indicated with square-dot line).

Fig.5: A field dependent sweep at the droplet onset current of -5.6 mA.

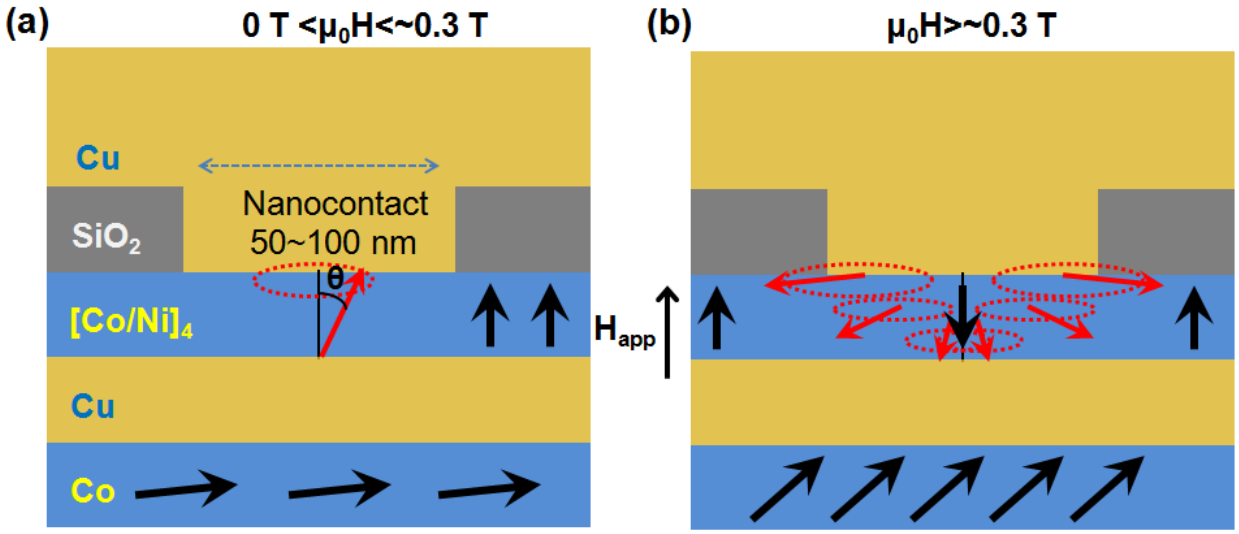

Fig.1, Mohseni et al.

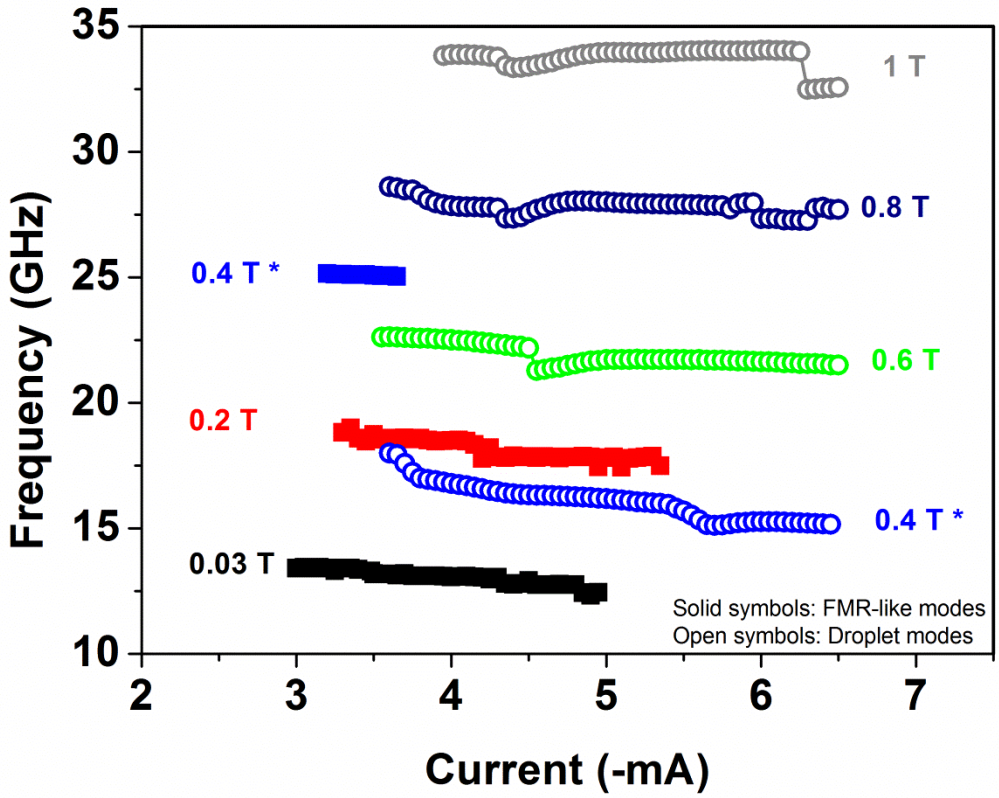

Fig.2, Mohseni et al.

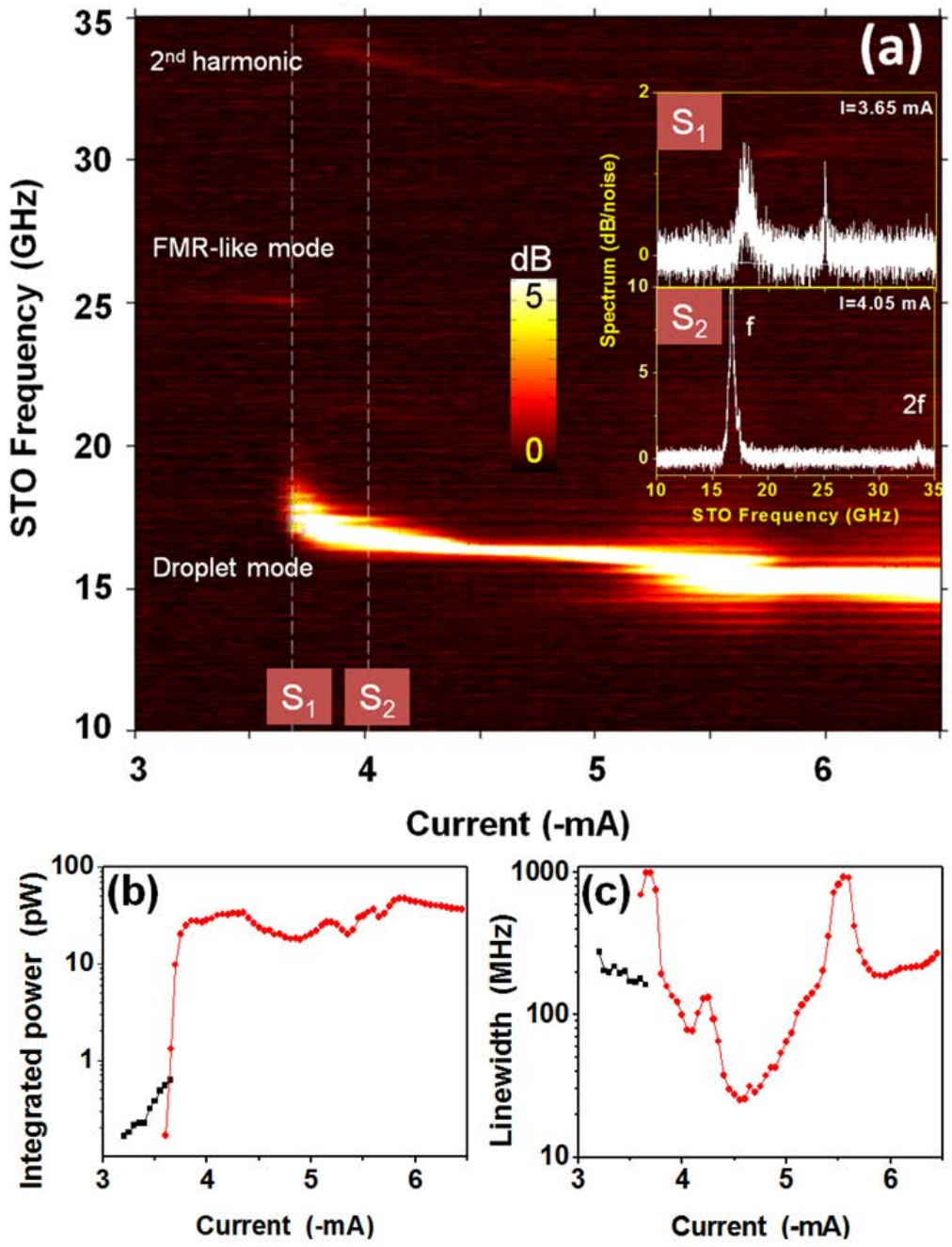

Fig.3, Mohseni et al.

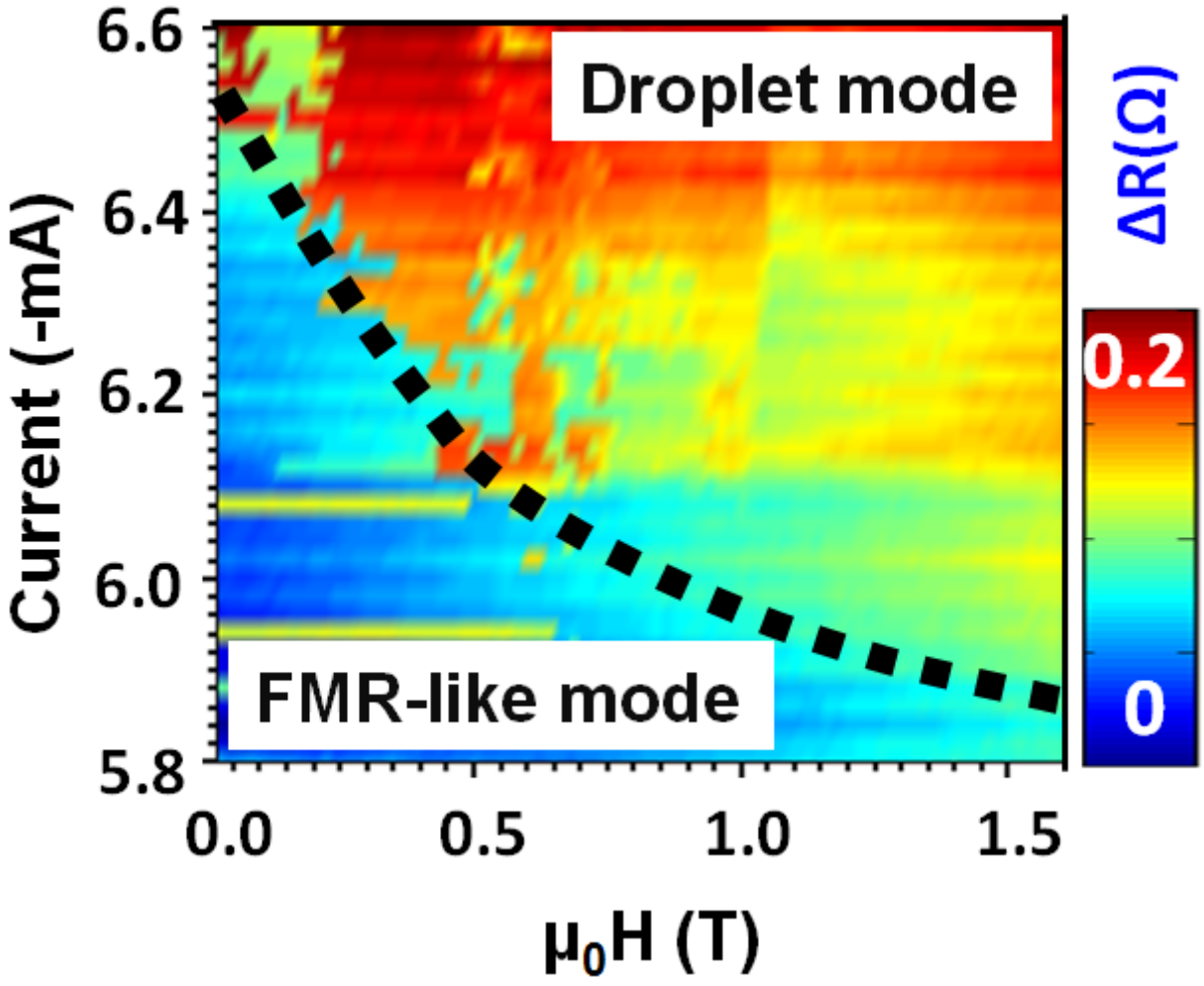

Fig.4, Mohseni et al.

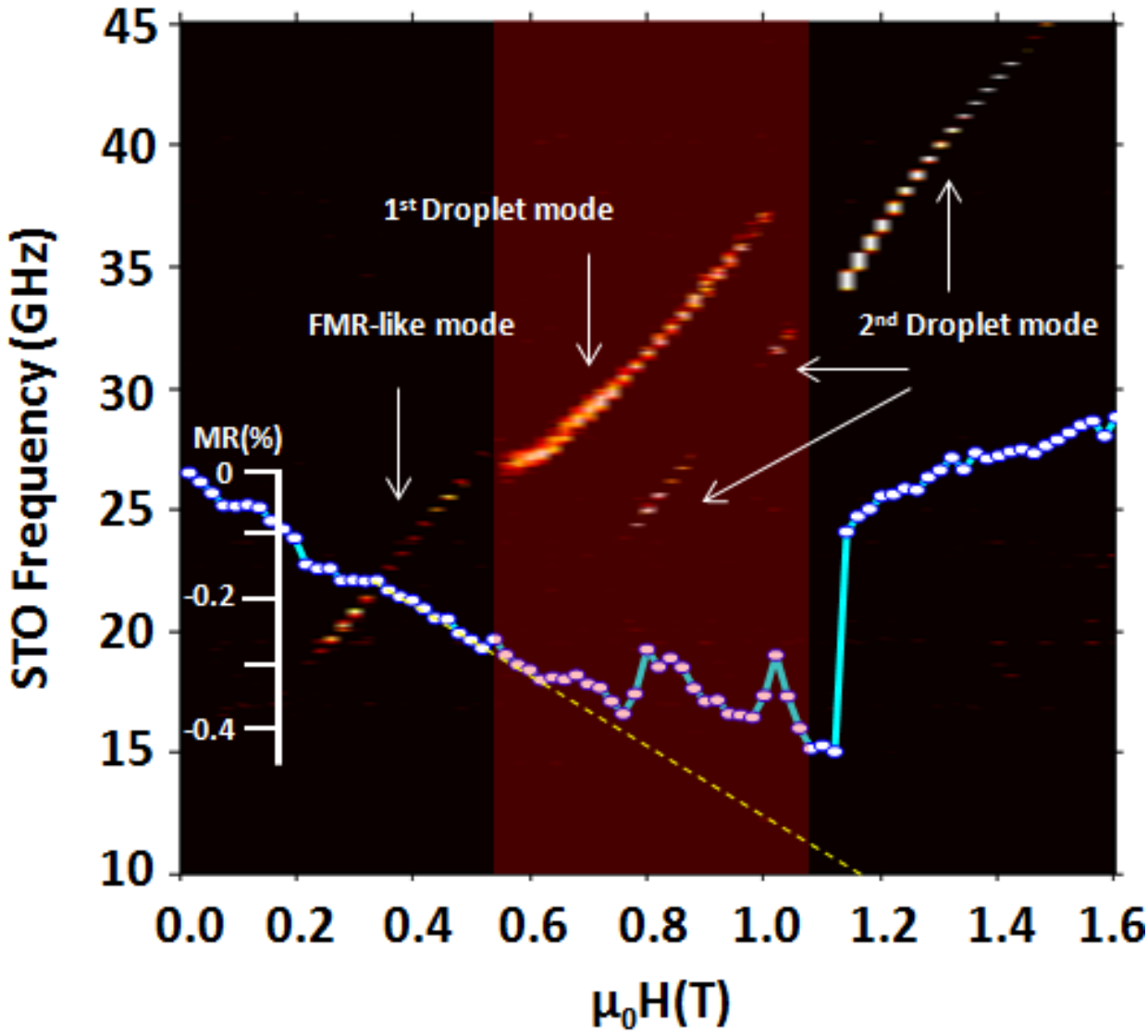

Fig.5, Mohseni et al.